Joule-heating effects in the amorphous $Fe_{40}Ni_{40}B_{20}$ alloy

P. Allia
Dipartimento di Fisica, Politecnico di Torino, Corso Duca degli Abruzzi 24, 10129 Torino, Italy

M. Baricco
Dipartimento di Chimica Inorganica, Chimica Fisica e Chimica dei Materiali, Università di Torino, Via Pietro Giuria 9, 10125 Torino, Italy

P. Tiberto
Dipartimento di Fisica, Politecnico di Torino, Corso Duca degli Abruzzi 24, 10129 Torino, Italy

F. Vinai
Istituto Elettrotecnico Nazionale "Galileo Ferraris," Corso Massimo D'Azeglio 42, 10125 Torino, Italy
(Received 18 February 1992; revised manuscript received 25 September 1992)

The effects of Joule heating on the amorphous $Fe_{40}Ni_{40}B_{20}$ alloy are investigated by measuring the time behavior of the electrical resistance of ribbon strips during such a treatment. The structural transformations occurring in subsequent stages of the process are studied by means of x-ray-diffraction, differential-scanning-calorimetry, and magnetic-permeability measurements. A continuous evolution from a fully amorphous to a fully crystalline structure may be followed. The crystallization mechanisms observed in Joule-heated samples differ from the ones occurring under conventional heating conditions. The electrical resistance displays a bump in the course of Joule heating. A quantitative model relating such a bump to the extra heat released to the sample by fast crystallization is proposed and discussed.

I. INTRODUCTION

Fast-heating techniques have been recently introduced in order to obtain metallic materials with attractive physical properties starting from amorphous ribbons. The soft magnetic properties of amorphous ferromagnets are improved by low-temperature anneals producing a relaxation of the atomic structure and a reduction in the level of quenched-in internal stresses.[1] The development of a dominant crystalline fraction in thermal treatments at higher temperatures generally destroys the soft magnetic properties of amorphous alloys.[2] Recently, however, the soft magnetic properties of certain Fe-based alloys have been shown to be improved by early crystallization stages, occurring at the sample surfaces during structural relaxation.[3]

Joule-heating of a metallic material essentially consists in submitting the metal to an electrical current of great intensity for a short time. This method has been successfully adopted to improve the magnetic properties of ferromagnetic amorphous alloys with negligible changes in their mechanical properties.[4–6] Joule-heating of Fe-B-Si amorphous ribbons leads to lower magnetic core losses[7] and lower coercive field[8] with respect to furnace annealing. Several current pulses of about 100 ms reduce coercive field in $Fe_{40}Ni_{40}B_{20}$.[9]

This technique is generally based on rather high heating rates (values up to 10^4–10^6 K/s under currents of the order 10 A have been reported[10]), allowing a sample to be crystallized at higher temperatures with respect to conventional techniques [typical heating rates in differential-scanning-calorimetry (DSC) measurements: 0.1–1 K/s]. A change in the crystallization products has been observed in Fe-Ni-Si-B amorphous ribbons by varying the heating conditions from DSC to Joule heating.[11,12] Finally, electrical current treatments have been used to study the kinetics of structural relaxation in CuTi amorphous alloys at low temperatures.[13]

Ultra-rapid Joule heating of metallic samples has proven to be particularly useful in advanced thermometry and pulse calorimetry, where the technique is exploited to perform measurements of specific properties, like the specific heat[14] and the emispherical emittance.[15]

Almost all papers dealing with Joule heating of metallic glasses are mainly concerned with its effects on various physical and structural properties. Specific studies of the evolution of these properties in the very course of this thermal treatment are still lacking. In our opinion, however, a better knowledge of the features of the process may provide valuable information about crystallization phenomena in metallic glasses. Moreover, many peculiar aspects of Joule heating of amorphous ribbons require an effort towards a deeper understanding of this process through on-line measurements.

Aim of this paper is to study the process of Joule heating in $Fe_{40}Ni_{40}B_{20}$, whose soft magnetic properties may be improved by such a treatment. The time scale of the process is made suitable for on-line physical measurements by using an electrical current of comparatively low intensity (of the order 1 A). Although in this case the heating rate is clearly lower than the maximum values quoted above, it remains higher by more than two orders of magnitude with respect to conventional annealing treatments. In this way, sample crystallization typically

occurs several seconds after a steady-state temperature distribution has been established in the sample, allowing one to perform proper measurements of selected physical properties before, during and after the crystallization process. In this paper, sample heating and subsequent crystallization have been monitored by measuring electrical resistivity changes.

II. EXPERIMENTAL TECHNIQUES

Amorphous $Fe_{40}Ni_{40}B_{20}$ has been produced in ribbon form by planar flow casting in air (average ribbon thickness $d=2\times10^{-5}$ m, width $l=5\times10^{-3}$ m. The samples used in electrical resistivity measurements were ribbon strips (length $L=0.1$ m) clamped at both ends by two couples of massive copper blocks of high thermal capacity, providing the electrical connections. A constant electric current was applied to the samples for times ranging from 10 to 20 s. The intensity of the electrical current ranged between 1.86 and 1.89 A, depending on sample resistance, in order to provide the same initial Joule power to all specimens. All treatments have been performed in vacuum in order to avoid sample oxidation and to reduce spurious conduction losses. The sample resistance was routinely measured before and after each treatment by means of a four-probe d.c. technique. The resistance variations were followed during the thermal treatments by simultaneously detecting the voltage across the sample and the electrical current flowing in it. The latter was obtained by measuring the voltage across a reference resistor of 0.21 Ω kept at room temperature. The resistivity changes observed in closely identical samples submitted to the same currents may be slightly different, owing to the inhomogeneity of different ribbon segments, attributable to small variations in thickness and surface defects (e.g., holes, quenched-in crystalline nuclei).

The structure of the samples has been checked by x-ray diffraction (Co$K\alpha$). Phase transformations have been studied by DSC (Perkin Elmer DSC7) in continuous argon flow at the constant heating rate of 0.5 K/s.

The room-temperature magnetic permeability μ_i of Joule-heated samples has been measured at 1 kHz by means of a conventional compensated-coil setup. The magnetic induction values did not exceed 1×10^{-3} T during the measurements.

III. SAMPLE HEATING: A SIMPLIFIED MODEL

In the unidimensional approximation, the sample temperature $T(x,t)$ satisfies a differential equation of the type[16]

$$\chi\frac{\partial^2 T}{\partial x^2}+B-\mathcal{L}(T)=C_p\frac{\partial T}{\partial t}\ , \tag{1}$$

where x is the distance measured along the sample's axis ($0\le x\le L$), χ is the thermal conductivity, B is the homogeneous Joule power density, $\mathcal{L}(T)$ represents the total power loss per unit volume, C_p is the product of the specific heat at constant pressure times the density. The Joule power density may be written as $B=I^2\rho/S^2$, ρ being the alloy's electrical resistivity, I the electrical current, and S the sample's cross section. Although χ, C_p, and ρ are temperature-dependent parameters, they will be considered as constant in a first approximation. The Thomson effect,[16] involving a term proportional to $\partial T/\partial x$ in Eq. (1), is neglected in the present treatment.

In ribbon strips characterized by very high surface-to-volume ratios (of the order 8×10^4 m^{-1}) and kept in vacuo, the dominant power-loss contribution arises from thermal radiation. Ideal thermal conduction towards the clamping copper blocks is accounted for by the usual boundary conditions, $T(0,t)=T(L,t)=T_0$, T_0 being room temperature. The radiation term may be written:[17]

$$\mathcal{L}(T)=P(T^4-T_0^4)\ , \tag{2}$$

where $P=2(1/L+1/l+1/d)\epsilon\sigma$, L, l, and d being sample length, width, and thickness, respectively, ϵ the alloy's hemispherical emittance, and σ the Stefan-Boltzmann constant.

The steady-state temperature profile is obtained by solving the equation

$$\chi\frac{d^2T}{dx^2}+B-P(T^4-T_0^4)=0\ . \tag{3}$$

When appropriate values are inserted for the parameters B and P, the numerical solutions of Eq. (3) turn out to be extremely flat functions of x over the greatest part of the interval $0\le x\le L$. In fact, the sample temperature may be considered essentially the same ($T_{\max}$) in the entire interval $0.1L\le x\le 0.9L$. Such a feature is strictly related to the relevant role played in this case by the radiation loss, even at the relatively low temperatures involved in the present measurements ($T\le 800$ K).

This circumstance grants validity to Joule heating as an alternative annealing technique of amorphous metallic alloys. In fact, the temperature turns out to always be homogeneously distributed within the sample (both ends excepted), therefore giving rise to a uniform thermal treatment on the considered sample.

The peculiar features of the exact solution of Eq. (3) justify neglecting the $\chi\partial^2T/\partial x^2$ term with respect to the other terms in that equation. Note that in amorphous alloys χ is rather small, of the order 10 W m^{-1}K^{-1}.[10] $T_{\max}$ may therefore be just obtained as

$$T_{\max}=(T_0^4+B/P)^{1/4}\ . \tag{4}$$

Equation (4) represents a very good approximation to the actual temperature profile of the sample far from both sample ends, because it provides a $T_{\max}$ value very close to the exact solution of Eq. (3) (less than 0.1 K) and never differing from the exact $T(x)$ value by more than 5 K over the entire interval $0.1L\le x\le 0.9L$. An experimental value for $T_{\max}$ may be deduced by considering the relative increase in the measured resistance R with respect to the room-temperature value R_0, $(R-R_0)/R_0\equiv\Delta R/R_0$. By admitting a linear dependence of resistivity on absolute temperature, one gets

$$(T_{\max})=T_0+\frac{(\Delta R/R_0)}{\alpha}\ , \tag{5}$$

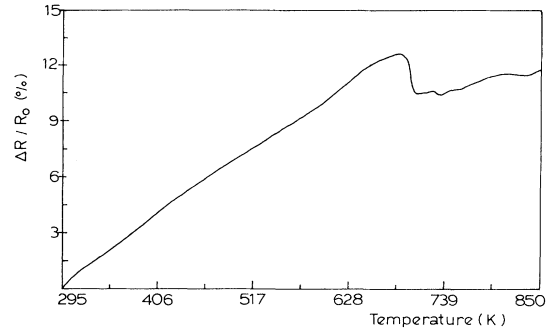

FIG. 1. Behavior of the reduced electrical resistance, $\Delta R/R_0 \equiv [R(T)-R_0]/R_0$ of a $Fe_{40}Ni_{40}B_{20}$ sample as a function of temperature. Heating rate 0.1 K/s. R_0 is the room-temperature resistance value.

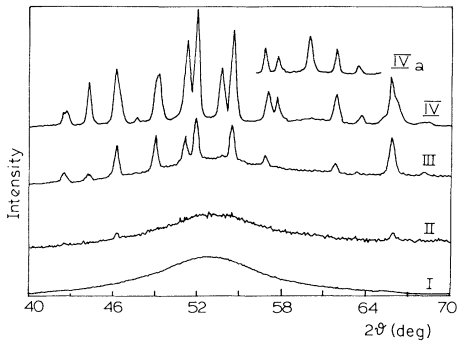

FIG. 3. X-ray diffraction patterns of selected $Fe_{40}Ni_{40}B_{20}$ samples submitted to Joule heating. Curve IVa refers to sample IV heated up to 873 K in DSC.

α being the alloy's temperature coefficient of resistance (TCR).

IV. RESULTS

The relative variation of the electrical resistivity of $Fe_{40}Ni_{40}B_{20}$ at constant heating rate (0.1 K/s), $\Delta R/R_0 \equiv \Delta\rho/\rho_0$, is shown in Fig. 1. The temperature drop marks the onset of crystallization. The TCR of the amorphous phase turns out to be $\alpha = 3\times10^{-4}\ K^{-1}$.

Figure 2 shows the typical behavior of the relative variation of resistance with respect to the room-temperature value, $\Delta R(t)/R_0$, as a function of Joule-heating time for an applied current of 1.88 A. The resistance is first observed to rapidly increase, owing to the fast sample heating from room temperature. Subsequently, a definite resistance plateau characterizes the occurrence of a steady-state temperature distribution inside the sample. After a given time, a well-defined resistance bump is observed. The maximum is followed by a continuous resistance decay until a constant value is reached. The final plateau corresponds to a resistance value appreciably lower than the first one. A quantitative analysis of this behavior will be performed in Sec. V A.

The x-ray diffraction patterns of various samples are shown in Fig. 3. The set of samples was obtained by interrupting the electrical current flow at the times marked by arrows in Fig. 2. It should be explicitly noted that in free cooling after the current break, the sample remains at high temperatures for a non-negligible time. The pattern of sample I shows the typical halo of a fully amorphous structure, without any appreciable modifications with respect to the pattern corresponding to the as-quenched sample. In sample II, two very small diffraction peaks may be observed. In sample III, the presence of a crystalline phase formed during free cooling immediately after the current break is evidenced by diffraction peaks superimposed to the broad halo of the remaining amorphous phase. By increasing Joule-heating time, a fully crystalline phase is produced, as shown by the diffraction pattern of sample IV. The diffraction peaks of the crystalline phase can be assigned to the orthorhombic $(Fe,Ni)_3B$ phase in all samples. No other phases appear in the x-ray diffraction measurements. By considering the entire set of Joule-heated samples for times ranging from before the start of the resistance peak

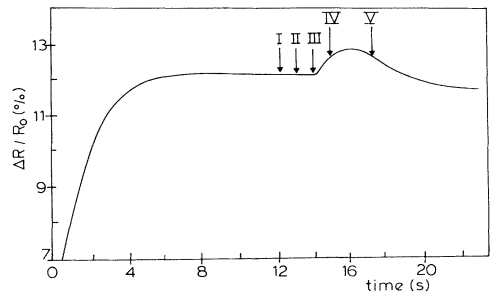

FIG. 2. Relative variation of the electrical resistance as a function of Joule-heating time in a $Fe_{40}Ni_{40}B_{20}$ sample. R_0 is the room-temperature resistance. Electrical current $I = 1.88$ A. The arrows indicate the treatment time of the various samples considered in the present study.

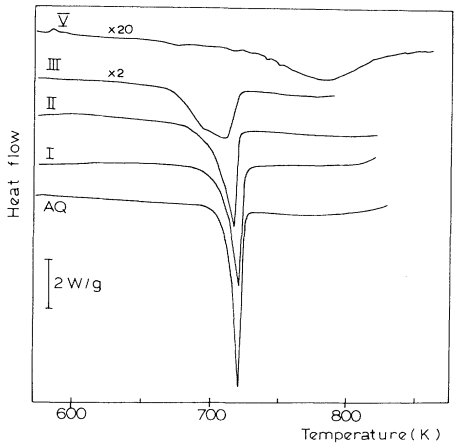

FIG. 4. DSC traces of phase transformations in selected $Fe_{40}Ni_{40}B_{20}$ samples as functions of temperature. AQ: as-quenched sample.

TABLE I. Onset temperature and heat of transformation.

Sample no.	T (K)	ΔH (kJ/mol)
As quenched	709	5.5
I	706	5.5
II	702	5.4
III	673	3.1
V	733	0.3

to well after, a continuous evolution from a fully amorphous to a fully crystalline phase may be followed.

The thermal stability of Joule-heated samples has been studied by DSC. The exothermic signals corresponding to phase transformations in the same samples studied through x-ray diffraction are shown in Fig. 4. The total heat released during the transformation and the corresponding onset temperature are reported in Table I.

The initial magnetic permeability of heat-treated samples, measured at room temperature and at $f=1$ kHz, and normalized with respect to the value of the as-quenched material, is reported in Fig. 5 as a function of Joule-heating time. The permeability value of a sample conventionally annealed at $T=723$ K for 2 h in controlled atmosphere is also reported for comparison (sample VI).

It should be noted that samples IV and V display almost indistinguishable x-ray diffraction patterns, DSC thermograms, and magnetic-permeability values.

V. DISCUSSION

The sample temperature T_{max} may be evaluated through Eq. (5). By taking $\Delta R/R_0=0.12$ (see Fig. 2), $\alpha=3\times10^{-4}$ K^{-1}, $T_0=300$ K, Eq. (5) provides $T_{max}=700$ K. A comparison between Eqs. (4) and (5) then gives $P=1.98\times10^{-3}$ W K^{-4} m^{-3} when $I=1.88$ A, $\rho=1.3\times10^{-6}$ Ω m, $S=1.0\times10^{-7}$ m^2, $B=4.6\times10^8$ J s^{-1} m^{-3}. This result for P corresponds to $\epsilon=0.35$, a reasonable value for the present alloy, lying between the average emittance of polished iron ($\epsilon\approx0.15$) and nickel ($\epsilon\approx0.15$) at $T\approx700$ K and the one of the oxidized metals at the same temperature ($\epsilon\approx0.6$ and $\epsilon\approx0.4$, respectively).[18]

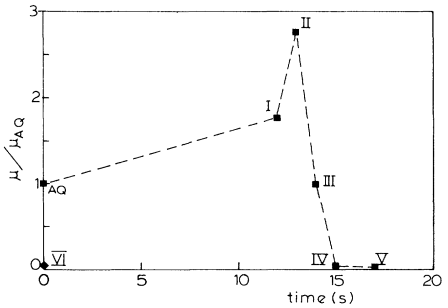

FIG. 5. Relative initial magnetic permeability of the $Fe_{40}Ni_{40}B_{20}$ alloy as a function of Joule heating time. μ_{AQ} is the initial magnetic permeability of the as-quenched material. AQ: as-quenched sample. Sample VI has been conventionally annealed (2 h at $T=723$ K).

A. A simple model of the resistance bump

Usually, the electrical resistance of metallic glasses is observed to drop during sample crystallization, although a few exceptions, including transition metal-metalloid glasses, exist.[19,20] The resistivity drop may be exploited to accurately determine the crystallization temperature.[21] When amorphous $Fe_{40}Ni_{40}B_{20}$ undergoes crystallization in conventional temperature scans at low heating rates, a drop in the electrical resistivity is indeed observed, as shown in Fig. 1. A closely similar curve for the same alloy is reported by Scott,[21] together with a DSC scan clearly showing that the resistivity drop is to be associated to crystallization.

Under Joule-heating conditions, however, the alloy's resistance-time curves display the bump reported in Fig. 2. Such a structure is clearly related to crystallization, as indicated by the x-ray diffraction patterns described above (Fig. 3). As a matter of fact, the same crystallization products were always observed in samples taken at different stages of the resistance bump. In the light of these results, the hypothesis of a development of transient crystalline products, somehow increasing the electrical resistance of Joule-heated samples, can be dropped. On the other hand, we will show that under reasonable assumptions the observed anomaly in the resistance-time curves may be explained by invoking a purely thermal mechanism, related to the extra-heat released to the sample during crystallization.

According to this hypothesis, crystallization, an exothermal phase transformation, gives rise to an increase in the average temperature of the sample, with a consequent increase in the resistance value, which enhances in turn the Joule-heating effect because the applied current is constant. As a result, the temperature is again slightly increased. Sample crystallization acts as a competing process, simultaneously producing a reduction in the resistivity of the material, as during conventional crystallization. The final sample temperature results from the balance between applied power and dissipation effects in the fully crystallized sample.

The model is made manageable by introducing some simplifying hypotheses. All structure-dependent parameters like α and C_p are kept constant. Also the hemispherical emittance is considered to stay constant during the entire treatment. The sample temperature and resistivity are assumed to be independent of the position x along the sample axis. As previously discussed, this approximation for T is always very good, with the exception of both ribbon ends, whose contributions are therefore neglected in the following. The homogeneous sample temperature is T_{max} defined in Eq. (4). In principle, a more accurate picture of the process may be provided, at the expense of a loss of simplicity and pregnancy of the model.

Let us introduce a new time scale, whose zero is coincident with the onset of the crystallization process at the temperature T_{max}. For $t\leq0$, we assume $R(t)=R_i$, $T(t)=T_{max}$, R_i being the steady-state resistance value of the heated amorphous sample.

The variations of resistance and temperature with respect to the initial values are $\Delta R(t)=R(t)-R_i$ and

$\Delta T(t)=T(t)-T_{\max}$. Let $f(t)$ be the developing crystalline fraction ($0\le f(t)\le 1$). Clearly, $\Delta R(0)=\Delta T(0)=f(0)=0$. $R(t)$ satisfies to the equation

$$\frac{dR}{dt}=\left[\frac{\partial R}{\partial T}\right]_f\frac{dT}{dt}+\left[\frac{\partial R}{\partial f}\right]_T\frac{df}{dt}=\alpha_r\frac{dT}{dt}-\gamma\frac{df}{dt}\ , \tag{6}$$

where γ has been defined as positive when the resistivity drops with increasing f, as usual.

Starting from $t=0$, an additional amount of energy per unit time is homogeneously released to the sample by the crystallization process. The additional power density W_f (expressed in W/m^3) may be written as

$$W_f=\Delta H_{\text{eff}}\frac{df}{dt}\ , \tag{7}$$

where ΔH_{eff} is the amount of the total density of crystallization heat effectively contributing to the extra heating of the sample. The temperature variation may be generally written as

$$C_p\frac{dT}{dt}=B+\Delta B-P(T^4-T_0^4)+W_f(t)\ , \tag{8}$$

where the term proportional to the spatial second derivative of T has been dropped, as before, and the term $\Delta B(t)$ accounts for the variation in B related to the resistance change resulting from the temperature drift: $\Delta B=I^2/(SL)\Delta R(t)$. Rewriting Eq. (8) in terms of ΔT, one gets (when $\Delta T\ll T_{\max}$)

$$C_p\frac{d(\Delta T)}{dt}=\frac{I^2}{SL}\Delta R-4PT_{\max}^3\Delta T+\Delta H_{\text{eff}}\frac{df}{dt}\ , \tag{9}$$

where use has been done of Eq. (4). The temperature and resistance variations satisfy therefore to the coupled equations (6) and (9). Equation (6) may be immediately integrated, giving

$$\Delta R=\alpha_r\Delta T-\gamma f\ , \tag{10}$$

the integration constant being zero. Let us define an effective time constant of heating, $\tau_h=C_p/(4PT_{\max}^3)$. The dependence of sample temperature on the resistance change is accounted for by:

$$\beta=\left(\frac{\partial T_m}{\partial R}\right)_f=\frac{I^2}{4SLPT_{\max}^3}\ . \tag{11}$$

The term $I^2/(SLC_p)$ may be therefore written as β/τ_h. By inserting Eq. (10) into Eq. (9), one gets

$$\frac{d\Delta T}{dt}+\frac{(1-\alpha_r\beta)}{\tau_h}\Delta T=\frac{\Delta H_{\text{eff}}}{C_p}\frac{df}{dt}-\frac{\beta\gamma}{\tau_h}f(t)\ . \tag{12}$$

The solution for ΔT may be written as

$$\Delta T=\frac{\Delta H_{\text{eff}}}{C_p}f(t)-\frac{[(\Delta H_{\text{eff}}/C_p)(1-\alpha_r\beta)+\beta\gamma]}{\tau_h}\times e^{-\lambda t}\int_0^t f(t')e^{\lambda t'}dt'\ , \tag{13}$$

where $\lambda=(1-\alpha_r\beta)/\tau_h$.

The time evolution of the electrical resistance is therefore given by

$$R(t)=R_i+\left[\frac{\alpha_r\Delta H_{\text{eff}}}{C_p}-\gamma\right]-\alpha_r\frac{[(\Delta H_{\text{eff}}/C_p)(1-\alpha_r\beta)+\beta\gamma]}{\tau_h}\times e^{-\lambda t}\int_0^t f(t')e^{\lambda t'}dt'\ . \tag{14}$$

It may be easily verified that for $t\to\infty$ the expressions for ΔT and $R(t)$ become

$$\Delta T_f=-\frac{\beta\gamma}{1-\alpha_r\beta} \tag{15}$$

and

$$R_f=R_i-\frac{\gamma}{1-\alpha_r\beta}\ . \tag{16}$$

The product $\alpha_r\beta$ is always much smaller than unity in all amorphous metallic alloys under realistic experimental conditions, so that no divergence of the right-hand terms of the previous expressions is actually expected. In fact, by using Eqs. (4) and (11), the product $\alpha_r\beta$ may be written (in the high-temperature, high-current limit) as $\alpha_r\beta\approx\frac{1}{4}\alpha T_{\max}$, which is always small because typical TCR's of amorphous metallic alloys lie in the 10^{-4} K^{-1} range,[22] and $T_{\max}$ cannot exceed the alloy's melting temperature (always in the 10^3 K range). It should be noted that R_f is expected to be lower than R_i in all amorphous metals where isothermal crystallization reduces the resistivity value.

Equations (13) and (14) allow one to picture the temperature and resistivity changes of the alloy from a knowledge of the evolving crystalline fraction, $f(t)$. The usual Johnson-Mehl-Avrami (JMA) expression for $f(t)$ (Ref. 23) is adopted

$$f(t)=1-e^{-(kt)^n}\ , \tag{17}$$

where k and n are constants to be determined. Strictly speaking, a JMA expression is not an appropriate kinetic law when sample temperature is changing, because the parameter k, containing the activation energy of the transformation, clearly depends on T. A constant value of k may be an acceptable assumption in the light of the previous approximations. On the other hand, the analysis of crystallization of $Fe_4Ni_{40}B_{20}$ in DSC cannot provide direct information on the values of k and n describing the kinetics of crystallization in Joule-heated samples, because different crystalline products are obtained through the two processes, as discussed in Sec. V D.

The resistance behavior of Joule-heated $Fe_{40}Ni_{40}B_{20}$ has been obtained by inserting the appropriate values of the various quantities appearing in Eq. (14). The parameter γ could be obtained in principle by measuring a resistance decay in isothermal conditions at $T=T_{\max}$; according to Eq. (16), however, it may also be obtained from the present experiment as

$$\gamma=(R_i-R_f)(1-\alpha_r\beta)\ . \tag{18}$$

By using $\alpha_r=\alpha R_i=4.1\times10^{-4}$ Ω/K, $\beta=130$ K/Ω, $\Delta H_{\rm eff}=3.2\times10^8$ J/m^3 ($\approx$2600 J/mol), $C_p=3.7\times10^6$ J/m^3 K ($\approx$30 J/mol K), $\gamma=6.6\times10^{-3}$ Ω, $\tau_h=1.36$ s, and by considering the JMA coefficients k and n as adjustable parameters, we obtain the curve of Fig. 6 (full line). Selected experimental values (open symbols) from Fig. 2 are superimposed to the theoretical curve, which corresponds to the choice $k=0.655$ s^{-1} and $n=1.5$.

The estimated temperature variation derived from Eq. (13) is reported in Fig. 7. Note that the maximum temperature variation predicted by the model amounts to about 35 K. As a consequence, the JMA rate k is significantly varied during the transformation. By assuming that the activation energy for crystallization be of the order 2 eV/at in the considered alloy, k turns out to be larger by a factor of about 5 at the top of the curve of Fig. 7 with respect to the beginning of the transformation. As a consequence, Eq. (17) should be substituted in an improved theory by a more complex expression, explicitly taking into account the occurrence of nonisothermal conditions. In our opinion, however, the model in the present form provides a simple, handy approach to the problem, giving a reasonably correct picture of the entire process.

The best-fit value of $\Delta H_{\rm eff}$ requires some comments. In fact, only a fraction of the total energy released during crystallization is expected to effectively contribute in the temperature rise of the sample. Owing to the reduced sample thickness and to its high surface-to-volume ratio, a non-negligible fraction of the total crystallization energy is immediately emitted instead of being absorbed by the sample. On the other hand, the total heat of crystallization ΔH, measured by DSC and reported in Table I, is actually the sum of $\Delta H_{\rm eff}$, and the heat generated in the calorimeter cell by conversion of the energy emitted by the sample. It is therefore not surprising that the best choice for $\Delta H_{\rm eff}$($\approx$2.6 kJ/mol) is found to be sensibly lower than the measured value of ΔH ($\approx$5.5 kJ/mol).

The agreement between the predictions of the model (even in the present simplified version) and the experimental data supports the hypothesis that the resistance

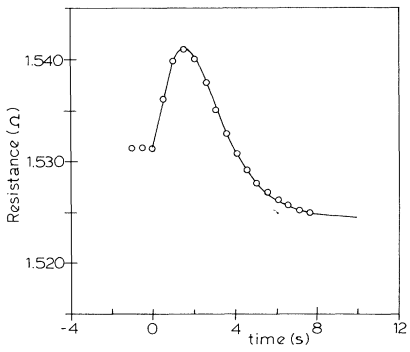

FIG. 6. Electrical resistance bump associated to crystallization of a Joule-heated sample. Circles: experimental data (see Fig. 2). Full line: theory. The zero of the time scale corresponds to the start of the bump.

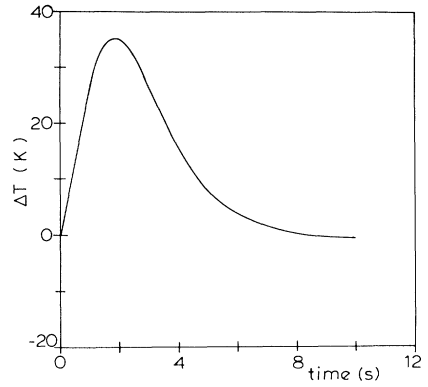

Fig. 7. Estimated temperature variation $\Delta T=T-T_{\rm max}$ during crystallization of a Joule-heated sample. $T_{\rm max}=700$ K. Same time scale as in Fig. 6.

peak is related to a sample temperature change, rather than to other possible causes, like changes in the electronic mean free path, or enhanced electronic scattering effects by crystallites of critical size produced during the crystallization process.

B. X-ray diffraction and DSC

The x-ray diffraction patterns of the samples heated up to 873 K at 0.5 K shows the coexistence of a fcc (Fe,Ni) solid solution and of the orthorhombic $(Fe,Ni)_3B$. As an example, curve IVa of Fig. 3 evidences the (200) diffraction peak of the (Fe,Ni) solid solution in the x-ray diffraction pattern. The as-quenched sample crystallizes in a single process step, as shown by the single peak in the DSC signal in Fig. 4 (curve AQ). Similar results are obtained on samples I and II, with a small reduction in the onset crystallization temperature but without any appreciable change in the heat of crystallization (Table I). The presence of very small diffraction peaks (Fig. 3, curve II) associated with a reduction in the onset temperature (Table I) suggests that very early stages of crystallization have been obtained in the course of Joule heating of sample II. The small crystalline fraction, of composition $(Fe,Ni)_3B$, likely confined at the surfaces of the ribbons, appears to be preferentially oriented on (201) and (040) crystallographic planes. Sample III is characterized by a strong reduction in the heat and temperature of crystallization with respect to the as quenched material (see Table I) and by the presence of a shoulder in the lower-temperature side of the exothermal DSC peaks (Fig. 4). In sample IV, an exothermal signal is still recognizable. It occurs however at higher temperatures with respect to the crystallization peaks of all other samples, and its intensity is rather low (see Table I).

C. Magnetic permeability

As usual, structural relaxation of this alloy leads to a definite increase in the μ_i value (sample I). However, the strongest variation in μ_i, corresponding to a peak in the $\mu_i(t)$ curve, is observed in sample II, characterized by a

very small crystallized fraction (see Fig. 3). A significant improvement of the soft magnetic properties on Fe-based amorphous ribbons occurs indeed in conventionally heated samples where thin crystallized layers have developed on both free surfaces, leaving the bulk substantially amorphous.[3] It may be inferred that even in the present case the few crystallites present in sample II are preferentially distributed over the ribbon surface.

As far as crystallization proceeds, the initial magnetic permeability drops (sample III), to finally reduce to vanishingly small values (samples IV and V). Note that the crystalline phases observed in these samples are nonmagnetic at room temperature. The magnetic-permeability values of samples IV and V are comparable to the one of sample VI which has been conventionally annealed at $T=723$ K for 2 h.

D. Crystallization products

Different crystallization mechanisms have been hypothesized for the $(Fe_{0.5}Ni_{0.5})_{100-x}B_x$ amorphous alloys, depending on B content.[24] When $x=16$, a primary crystallization occurs, when $x=20$ two different phases crystallize with a eutectic reaction, and when $x=25$ a polimorphous phase transition is produced from the amorphous phase to crystalline $(Fe,Ni)_3B$. In amorphous $Fe_{40}Ni_{40}B_{20}$, annealing at temperatures below 673 K leads to the formation of orthorhombic $(Fe,Ni)_3B$ coexisting with an amorphous phase. The formation of a fcc (Fe,Ni) solid solution becomes evident only at higher temperatures.[25]

Various types of crystals have been put into evidence by TEM analysis of the early stages of crystallization in amorphous $Fe_{40}Ni_{40}B_{20}$. Eutectic fcc (Fe,Ni) + $(Fe,Ni)_3B$, eutectic fcc (Fe,Ni) + $(Fe,Ni)_{23}B_6$ and single-phase fcc (Fe,Ni) crystals have been found by some research groups.[26,27] In particular, TEM analysis of the microstructures formed upon annealing of as-quenched samples between 628 and 658 K (Ref. 26) indicates that both nucleation and growth are characterized by a specific behavior for each of the three crystalline products mentioned above. In fact, eutectic mixtures are shown to nucleate athermally, whereas the single-phase fcc (Fe,Ni) solid solution is characterized by a constant nucleation rate. In the considered temperature range, the eutectic mixture of fcc (Fe,Ni) + $(Fe,Ni)_3B$ displays a growth rate definitely higher than fcc (Fe,Ni) + $(Fe,Ni)_{23}B_6$, even if the activation energy for growth turns out to be the same.[26] In other cases, only small crystallites of $(Fe,Ni)_{23}B_6$ with embedded fcc (Fe,Ni) have been observed.[28]

The crystallization mechanism in $Fe_{40}Ni_{40}B_{20}$ seems also to be affected by the heating rate used during the heat treatment. From x-ray diffraction and DSC analysis of as-quenched and Joule-heated samples, three different crystallization mechanisms can be evidenced in the present case. In an as-quenched sample heated in DSC, eutectic crystallization of fcc (Fe,Ni) and of a $(Fe,Ni)_3B$ phase occurs, as previously reported.[24] In the partially crystallized sample (III), the formation of a $(Fe,Ni)_3B$ phase during the Joule treatment and subsequent free cooling leaves an amorphous phase slightly depleted in B. The crystallization of this amorphous phase has been subsequently observed in DSC. It occurs through a primary mechanism, evidenced by the shoulder of the DSC peak (Fig. 4, curve III). In sample IV, crystallization in the course of Joule heating produces mainly the $(Fe,Ni)_3B$ phase, suggesting a polimorphic mechanism. Further heating up to 873 K transforms the monophasic system by an exothermic precipitation reaction (Fig. 4, curve V) into a two-phase mixture consisting of fcc (Fe,Ni) and $(Fe,Ni)_3B$ phases (Fig. 3, curve IVa). A similar crystallization mechanism has been reported for the same system under different heating conditions.[29]

The occurrence of a polimorphic crystallization mechanism in the course of Joule heating of sample IV can be also deduced from the values of the lattice parameters of the orthorhombic phase $(Fe,Ni)_3B$. In sample IV, these are $a=5.31$ Å, $b=6.63$ Å, $c=4.43$ Å, whereas in an as-quenched sample heated up to 873 K at 0.5 K/s the lattice parameters are $a=5.35$ Å $b=6.65$ Å, $c=4.45$ Å. The orthorhombic $(Fe,Ni)_3B$ phase is likely to dissolve different B concentrations, as reported for the Fe_3B phase.[30] The lattice parameters are expected to depend on both B content and Fe/Ni ratio. When the Fe/Ni ratio can be considered to stay constant, as in the present case, the lattice parameters are expected to be lower for lower B content. If polimorphic crystallization occurs in $Fe_{40}Ni_{40}B_{20}$, a single-crystalline phase $(Fe,Ni)_3B$ with 20 at. % of B is expected, having consequently lower lattice parameters with respect to the stoichiometric compound. In fact, in sample IV, lower values of the lattice parameters have been obtained with respect to the ones corresponding to the $(Fe,Ni)_3B$ phase formed by a eutectic reaction during DSC heating of an as-quenched sample. The latter process is considered to give rise to the stoichiometric composition.

It is worth noting that, in the early stages of crystallization in DSC (as-quenched sample heated up to 713 K), only x-ray diffraction peaks of $(Fe,Ni)_3B$ can be evidenced, indicating that this phase is the dominant one during the early stages of crystallization, in agreement with previous results.[26] This observation suggests that crystallization of $Fe_{40}Ni_{40}B_{20}$ in DSC starts with the formation of $(Fe,Ni)_3B$ phase and goes on with the formation of the eutectic mixture. In the case of crystallization by Joule heating of sample IV, the very high heating rate forces the system into a single crystalline phase, a redistribution of the solute being substantially inhibited by kinetic reasons. The structure of the phase obtained by fast heating strongly depends on the growth rate. In the present case, the orthorhombic $(Fe,Ni)_3B$ phase, characterized by a high growth rate,[26] appears as the main crystallization product. A further anneal of this boride phase in DSC gives rise to the thermodynamically stable mixture of fcc (Fe,Ni) and $(Fe,Ni)_3B$ with the correct stoichiometry.

VI. CONCLUSIONS

In Joule-heating treatments, the sample temperature appears to be determined by radiative effects, constituting

the dominant energy-loss mechanism in thin samples, like amorphous ribbons, even at the relatively low temperatures of interest here. The resulting steady-state temperature profile is always very flat, thereby ensuring optimum conditions for a homogeneous heat treatment of the material.

It is suggested that the bump observed in resistance-time plots is related to the extra heat released to the sample in a very short time during quasi-isothermal crystallization. In conventional treatments, the same heat is released over a much longer time interval, and the bump disappears.

The anomalous heating conditions produced by this technique strongly affect the crystallization mechanisms. The crystallization products differ from the ones obtained by DSC heating. At low heating rates, as in DSC measurements, a eutectic crystallization of fcc (Fe,Ni) solid solution and orthorhombic $(Fe,Ni)_3B$ is observed. In the course of Joule heating, a polimorphic crystallization of $(Fe,Ni)_3B$ occurs instead, giving rise to a phase with lower B content with respect to the stoichiometric compound. Quantitative figures of the activation energy of the process cannot however be obtained from an analysis of the electrical-resistivity data, owing to the simplification introduced in the adopted model.

Also the initial permeability μ_i is significantly affected by Joule heating of the samples. A strong increase of μ_i is observed in the sample displaying a very small crystalline fraction, indicating that the crystallized phase essentially appears at the sample surfaces.

[1]F. E. Luborsky, in *Amorphous Metallic Alloys,* edited by F. E. Luborsky (Butterworths, London, 1983), p. 360.
[2]M. Baricco, F. Vinai, P. Allia, and C. Antonione, Philos. Mag. B **61**, 576 (1990).
[3]H. N. Ok and A. H. Morrish, Phys. Rev. B **22**, 3471 (1980).
[4]T. Jagielinski, IEEE Trans. Magn. **MAG-19**, 1225 (1983).
[5]D. R. Huang and J. C. M. Li, Scr. Met. Mat. **24**, 1137 (1990).
[6]P. Rougier and R. Krishnan, J. Phys. (Paris) Colloq. **46**, C6-417 (1985).
[7]A. R. Yavari, R. Barrue, M. Harmelin, and J. C. Perron, J. Magn. Magn. Mater. **69**, 43 (1987).
[8]T. Kulik and A. Matyja, Mater. Sci. Eng. A **133**, 232 (1991).
[9]M. R. J. Gibbs, D. H. Lee, and J. E. Evetts, IEEE Trans. Magn. **MAG-20**, 1373 (1984).
[10]A. Zaluska, D. Zaluski, R. Petryk, P. G. Zielinski, and H. Matyja, in *Proceedings of the Rapidly Quenched Metals 5,* edited by S. Steeb and H. Warlimont (Elsevier, Amsterdam, 1985), p. 235.
[11]A. Zaluska and H. Matyja, Int. J. Rapid Solidif. **2**, 205 (1986).
[12]L. Zaluski, A. Zaluska, M. Kopcewicz, and R. Schulz, J. Mater. Res. **6**, 1028 (1991).
[13]H. Mizubayashi and S. Okuda, Phys. Rev. B **40**, 8057 (1989).
[14]A. Cezairlyan, in *Specific Heat of Solids,* edited by C. Y. Ho (Hemisphere, New York, 1988), p. 323.
[15]F. Righini, G. C. Bussolino, and A. Rosso, Int. J. Thermophys. **13**, 17 (1992).
[16]J. Spisiak and F. Righini, Int. J. Thermophys. **13**, 29 (1992).
[17]K. D. Maglic and A. S. Dobrosavljevic, Int. J. Thermophys. **13**, 3 (1992).
[18]R. A. Matula, in *Properties of Selected Ferrous Alloying Elements,* edited by C. Y. Ho (Hemisphere, New York, 1989), pp. 120 and 198.
[19]H. S. Chen and D. Turnbull, J. Chem. Phys. **48**, 2560 (1968).
[20]R. Yokota, K. Matusita, Y. Shiraishi, M. Yoshida, and T. Komatsu, in *Proceedings of the 4th International Conference on Rapidly Quenched Metals,* edited by T. Masumoto and K. Suzuki (Japanese Institute of Metals, Sendai, 1982), Vol. 2, p. 1357.
[21]M. G. Scott, in *Amorphous Metallic Alloys,* edited by F. E. Luborsky (Butterworths, London, 1983), p. 144.
[22]U. Mizutani, Prog. Mat. Sci. **28**, 97 (1983).
[23]J. W. Christian, *The Theory of Transformations in Metals and Alloys* (Pergamon, Oxford, 1975), p. 15.
[24]U. Koster, Z. Metallkde **75**, 691 (1984).
[25]J. Cernak, M. Cernansky, P. Duhaj, and J. Horvath, Phys. Status Solidi (A) **91**, 407 (1991).
[26]K. Müller and M. von Heimendahl, J. Mater. Sci. **17**, 2525 (1982).
[27]V. S. Raja, Kishore, and S. Ranganathan, J. Mater. Sci. **25**, 4667 (1990).
[28]R. Gerling and R. Wagner, Scr. Metall. **17**, 1129 (1983).
[29]Y. Khan, Z. Metallkde **74**, 385 (1983).
[30]Y. Khan, E. Kneller, and M. Sostarich, Z. Metallkde **73**, 624 (1982).